Identification of Potential Ablation Targets for Ventricular Tachycardia Using a Novel Omnipolar-based Propagation Organization Metric

Samuel Ruipérez-Campillo[1,3], Gema Cabero[1], Johanna Tonko[2], José Millet[1], Pier Lambiase[2], Francisco Castells [1]

[1]ITACA Institute, Universitat Politécnica de Valencia, Valencia, Spain
[2]Institute for Cardiovascular Science, University College London, London, UK
[3 (current affiliation)] Department of Computer Science, ETH Zurich, Zurich, Switzerland

Abstract

The optimal approach to identify sites to target with ablation during ventricular substrate mapping for ventricular tachycardia (VT) remains debated. Our study aims to evaluate the diagnostic utility of a novel propagation organization metric, the omnipolar-based local vector field heterogeneity (VFH), to differentiate functionally critical sites from bystander areas during ventricular substrate mapping to inform ablation strategy. We compared VT isthmus sites, low-voltage bystander areas (LVAs), and normal voltage areas (NVAs). The substrate maps from nine patients were segmented by domain-experts according to these sites, and the VFH metric was calculated for each region. We performed statistical analyses of VFH values across the three sites, identifying statistically significant differences between each pair of regions ($p < 0.001$). The VFH mapping revealed a statistically significant increase in electrical heterogeneity at critical isthmus sites compared to LVAs and NVAs. The VFH metric is a promising new substrate mapping strategy to identify targets for catheter ablation in scar-related ventricular tachycardias.

1. Introduction

Ventricular tachycardia (VT) in patients with structural heart disease can be life-threatening and is most commonly secondary to a reentry mechanism [1]. Percutaneous catheter ablation is an established treatment modality to reduce the risk of VT recurrence and ICD shocks and has been proven to be more effective than medical therapy alone for this purpose [2].

Traditionally, activation and entrainment mapping of induced VTs have been proposed to identify critical sites to target with ablation. Yet, these approaches are frequently hampered by hemodynamic intolerance, unstable and/or changing VTs or non-inducibility [3].

Substrate mapping has emerged as an important alternative approach to characterize areas likely to support reentry based on electrophysiological characteristics that can be determined during stable sinus or paced rhythm. In previous studies, it has been suggested that this approach allows for the elimination of VT, irrespective of inducibility or hemodynamic tolerance. Some studies conclude that even for hemodynamically stable VTs, substrate mapping can be used to limit activation mapping or entrainment to a region of interest [4].

Detailed substrate characterization has been facilitated by widespread use and availability of high-density mapping technologies employing dedicated multipolar mapping catheters. Among these, the 16-pole HD Grid catheter has the advantage to offer a fixed electrode arrangement enabling uniform spatial sampling as well as the reconstruction of orientation-independent omnipolar EGMs (oEGMS), that have been reported to address some limitations of unipolar and bipolar EGMs [5]. Here we propose to apply recently developed heterogeneity metric based on intracardiac oEGMs to quantify and characterize abnormal propagation patterns and evaluate its clinical use during ventricular substrate mapping to identify targets for ablation.

2. Materials and Methods

Study cohort

A cohort of 9 patients (64±18 years) with scar related VT who underwent clinically indicated catheter ablation involving substrate and VT activation mapping was considered. 77.8% had an ischemic etiology. The average left ventricular ejection fraction (LVEF) was 33% (±10). On average, 4.3 VTs (range: 1-8) were induced per case.

Contact mapping

A 16-pole grid catheter with a 4x4 arrangement of 1-mm equidistant electrodes and 3-mm interelectrode spacing was used alongside the EnSite NavX system. This system enabled acquisition of high-density substrate maps and ventricular tachycardia (VT) activation maps from the patients with scar-related VT.

Critical sites were identified based on VT activation maps and confirmed by either entrainment or VT termination with radiofrequency (RF) ablation. Subsequently, the corresponding substrate maps were segmented into isthmus-site, low voltage bystander areas

(LVA, omnipolar voltage <1.5mV), and normal voltage areas (NVA, >1.5mV). The mean substrate map point count was 3825 ± 3190.

Pre-processing and activation window selection

Because unipolar EGMs can be very noisy due to common interferences such as far field, electromagnetic coupling, catheter handling and other interferences, a robust detection of the activation pulse is required. For this purpose, we employed a modified version of the so-called Botteron preprocessing steps, which firstly reduces noise outside the activation intervals by means of a Butterworth bandpass filter (6th order, [40 Hz to 250 Hz]), followed by a rectification and low-pass filter (6th order Butterworth, cut-off 20 Hz) acting as an envelope detector. This processing sequence significantly reduces signal dynamics, highlighting the energy of the activation amidst other interferences [6,7]. The window of interest is selected based on intervals of maximal energy across all 16 electrode recordings.

Propagation wavefront vector

The direction of the propagation wavefront is estimated at clique level from the representation of the electrical field loop. Considering each clique as a square 2x2 electrode arrangement, a pair of orthogonal bipolar EGMs (bEGMs) ***b1*** and ***b2*** is derived according to a cross-configuration scheme of the clique. Following this approach, the bEGMs are computed from the subtraction of the unfiltered uEGM activations from the electrode pairs corresponding to the diagonals of the clique. This configuration satisfies the condition of spatial coincidence of the bipole pair, hence avoiding time misalignments of the activations, which are prone to occur when using a triangular clique [7]**.** To project the signals onto the x-y coordinate system, a π/4 rad clockwise rotation is then applied to the diagonal bipoles:

$$\boldsymbol{b}(t) = \begin{bmatrix} \cos\left(\frac{\pi}{4}\right) & -\sin\left(\frac{\pi}{4}\right) \\ \sin\left(\frac{\pi}{4}\right) & \cos\left(\frac{\pi}{4}\right) \end{bmatrix} \cdot \begin{bmatrix} \boldsymbol{b}_1(t) \\ \boldsymbol{b}_2(t) \end{bmatrix} = \begin{bmatrix} \boldsymbol{b_x}(t) \\ \boldsymbol{b_y}(t) \end{bmatrix}$$

Over the course of a depolarization, the local E-field, formed by the perpendicular bipoles, bx – by, creates the so-called bipolar loop. The loop's greatest magnitude corresponds to the direction of wavefront propagation [8] and is indicated by a unitary vector Γ located at the clique's centre. This vector conforms an angle θ_o respect to the x-axis that is estimated according to the optimization function:

$$\theta_o = \underset{\theta}{\operatorname{argmax}} \left[\frac{\max([\cos\theta \quad -\sin\theta]\mathbf{b}(t))}{\max|[\sin\theta \quad \cos\theta]\mathbf{b}(t)|} \right]$$

The omnipolar EGM (oEGM) is then defined as the virtual bipole that would be obtained as if it would have been picked up from a pair of electrodes oriented in the direction of the propagation wavefront (see Figure 1). Accordingly, the oEGM es estimated as the projection of the E-field on the axis defined by the unitary vector Γ. The rotation that retrieves the oEGM *o(t)* is:

$$\begin{bmatrix} o(t) \\ r(t) \end{bmatrix} = \begin{bmatrix} \cos(\theta_o) & -\sin(\theta_o) \\ \sin(\theta_o) & \cos(\theta_o) \end{bmatrix} \mathbf{b}(t)$$

with *r(t)* being the residual component corresponding to the projection of the loop on an axis that is perpendicular to the direction of the propagation wavefront.

Vector Field Heterogeneity

For a 4 × 4 electrode grid and according to the definition of a clique, a 3 × 3 vector map is generated, displaying the propagation angle θo of the propagation wave on the tissue in contact with the catheter [9]. For each clique (*i,j*) the local vector field heterogeneity $\Psi_{i,j}$ was defined from the approximated partial derivatives which, in a discrete form was defined from the finite differences between its propagation vector $\mathbf{u}_p$ and the propagation vectors at its neighboring cliques:

$$(\Psi)_{i,j} = \frac{\left(\frac{\Delta\boldsymbol{\Gamma}}{\Delta x}\right)_{i,j} + \left(\frac{\Delta\boldsymbol{\Gamma}}{\Delta y}\right)_{i,j} + \frac{1}{\sqrt{2}}\left[\left(\frac{\Delta\boldsymbol{\Gamma}}{\Delta d_1}\right)_{i,j} + \left(\frac{\Delta\boldsymbol{\Gamma}}{\Delta d_2}\right)_{i,j}\right]}{(\xi)_{i,j}}$$

$$0 \le (\Psi)_{i,j} \le 1$$

which includes the finite differences not only from the horizontal and vertical axis, but also the diagonals d^1 (at π/4 rad) and d_2 (at 3π/4 rad). Notice a reduced weighting factor for the diagonal components as the diagonal neighbors are more distant. Moreover, also notice the scaling factor $\xi_{i,j}$ to correct boundary effects at the edges of the multielectrode since less neighbor cliques are available. Finally, the Vector Field Heterogeneity at multielectrode level is computed as an average of the heterogeneity at all cliques:

$$\mathrm{VFH} = \frac{\sum_{i=1}^{p}\sum_{j=1}^{q}(\Psi)_{i,j}}{p \cdot q} : 0 \le \mathrm{VFH} < 1$$

Statistical Analysis

To evaluate the performance of the VFH metric in the segmented regions, firstly we conducted pairwise comparisons using Welch's t-test, also known as the unequal variance t-test. The null hypothesis proposed that the VFH means between two regions are equal. Additionally, to control the Family Wise Error Rate (FWER), we applied the step-down Bonferroni procedure of Holm, correcting for multiple comparisons and providing multiplicity-adjusted values for significance. In addition, we employed Welch's alternative to one-way analysis of variance (ANOVA) to assess the equality of population means across the three different groups (isthmus, LVA, and NVA regions). Area under receiving operating characteristics curves (AUROC) were used to compare the VFH between regions. Data are presented as mean ±SD unless stated otherwise.

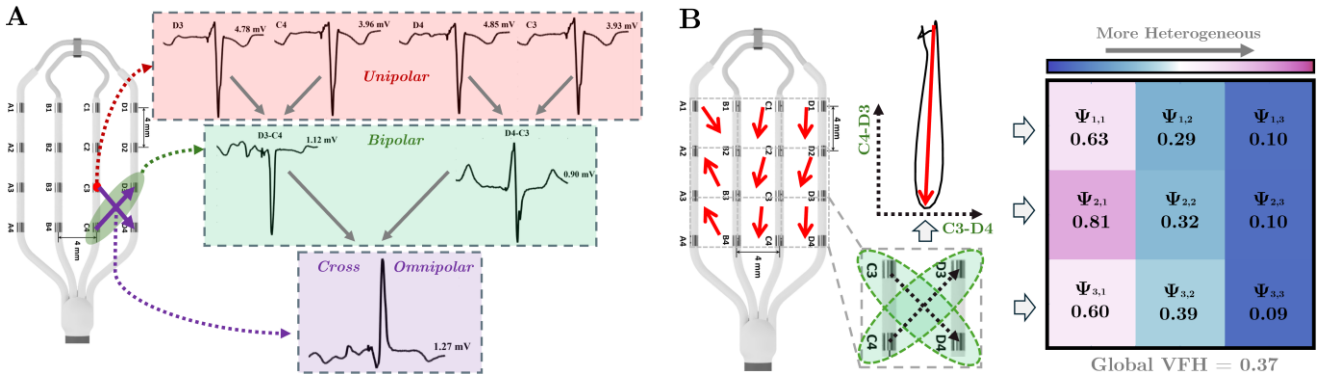

Figure 1. *Cross omnipolar reconstruction.* **A)** *Illustration of a cross-omnipole from unipoles in the voltage domain.* **B)** *Example of the propagation direction estimation from oEGMs and VFH map reconstruction.*

3. Results

The value for the local VFH metrics were 0.56 ± 0.22 at sites corresponding to VT isthmus regions, 0.47 ± 0.26 at LVA, and 0.30 ± 0.25 at NVA. VFH at isthmus sites showed significantly higher values, indicating more disorganization, compared to LVA bystander sites ($p<0.001$). Conversely, VFH was significantly lower in NVA, indicating more organization, compared to both isthmus and LVA sites ($p<0.001$). These results are depicted in Table 1 and illustrated in Figure 2 (upper panels). Additionally, the Welch's F test shows that the associated probability is <0.001, supporting the means to not be equal.

Table 1. Summary of mean and standard deviation of VFH values across different regions.

Region	Mean ± St. Dev	Median [IQR]
Isthmus	0.56 ± 0.22	0.58 [0.30]
LVA	0.47 ± 0.26	0.48 [0.39]
NVA	0.31 ± 0.25	0.22 [0.25]

Further, we evaluated the ability of the local VFH metric to discern between the isthmus vs NVA, and LVA vs NVA. For isthmus vs NVA regions, the VFH metric achieved an AUROC of 0.78 and an accuracy of 0.71 for the optimal threshold. In the task of delineating LVA from NVA, the AUROC was 0.68, and the accuracy was 0.65.

Additionally, qualitative examples of isthmus, NVAs and LVAs heterogeneity maps and their corresponding vector map for the cross-configuration are depicted in figure 2 (lower panel), alongside with a 3D VFH map for that case. Further, figure 3 depicts the local VFH values for the isthmus regions, LVA and NVA, along with the voltage maps for these regions in a VT patient (male, LVEF 25%).

4. Discussion

In this study, we propose, in the context of a clinically relevant scenario, the validation of the local VFH, a heterogeneity metric based on vector field analysis to characterize the local electrophysiological substrate.

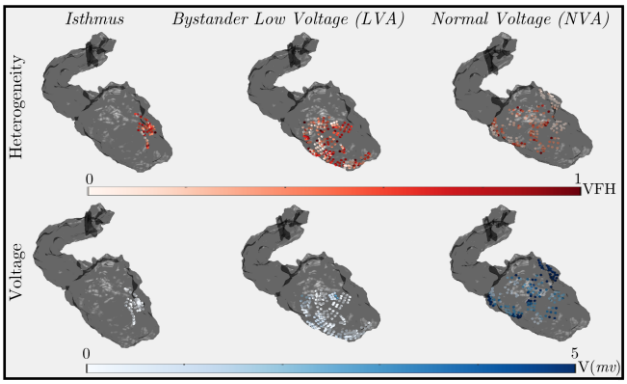

Figure 3. *Illustration of VFH maps together with voltage maps for a patient with VT (male 64 y.o., ICM, LVEF 25%)*

Applying this approach to a clinical intracardiac mapping dataset acquired during routine clinical catheter ablation procedures for scar related VT using standard multipolar grid catheters, we were able to demonstrate a statistically significant increase in electrical heterogeneity at sites corresponding to the critical isthmus of the VT compared to bystander sites in ventricular substate maps. This supports the clinical value of VFH as a novel mapping strategy to identify critical sites to target with ablation. The VFH metric parameter is computed from omnipolar-derived vector could easily be translated and integrated into commercial mapping systems and complement existing approaches. While there are works aiming to characterize the organization of wavefront propagation based on intracardiac recordings (e.g. REACT [10], RAAPs [11]), we proposed the first approach based on vector field theory generalizable intracardiac recordings on grid catheters. Other possible clinical applications of the VFH metric, could be the identification of focal or rotational patterns, training further algorithms that relate VFH values to propagation patterns.

As any diagnostic tool, the accuracy is fundamentally linked to the quality of the data and presence of confounders. Initial in-silico validation of computational advanced mapping approaches often relies on idealized conditions. Yet, electro anatomical mapping data acquired

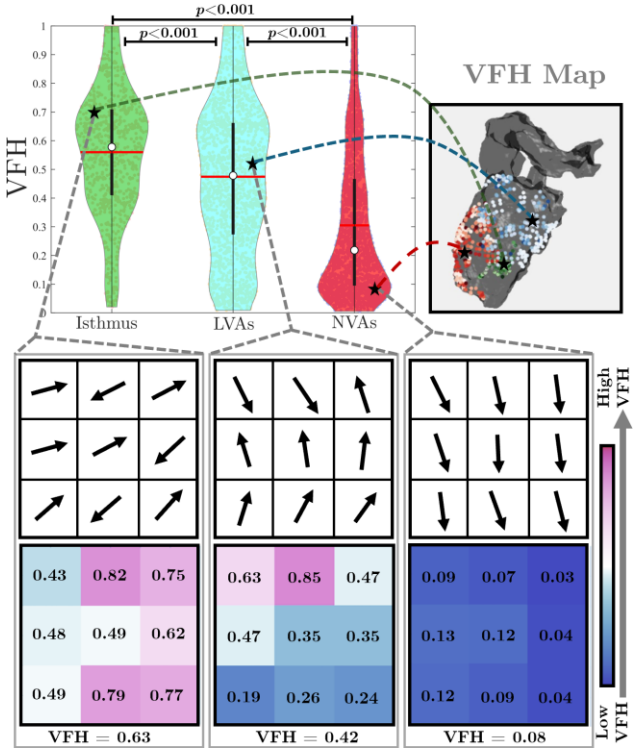

Figure 2. Upper panels: *summary Statistics and Data Distribution Boxplots for local VFH by region of interest in N=9 VT patient recordings. The shape of the box illustrates the density data distribution. The red line indicates the mean value of local VFH for each category. Black bold lines indicate the interquartile range and white dots represent the median of the distribution.* Lower Panels: *Illustration of a patient in VT. Local heterogeneity and vector maps for: NVA isthmus site (right), LVA (center), isthmus sites (left) alongside the corresponding VT activation maps.*

in the context of clinical VT ablation procedures, that need to prioritize safe and time-efficient delivery of ablation therapy, often deviates substantially. Besides the clinical condition of the patient, sequential contact mapping technology itself is inherently affected by numerous confounders: Catheter movement as well as insufficient electrode-tissue coupling ("poor contact"), far-field signals, iatrogenic extra beats and electrical noise and artefacts all can interfere with the acquisition of in vivo cardiac signals. On the epicardial surface, presence of epicardial adipose tissue may further impact the EGM morphology. Lastly, the restriction to surface mapping does not allow to estimate the true complexity of the ventricular activation wavefronts in structurally abnormal hearts. On top of these, there are technical challenges such as the lack of ground truth to detect activation intervals in intracardiac signals, which may affect the computation of bipolar loops and the propagation direction estimation. Interpretating the diagnostic accuracy of the VFH metric for ventricular substrate mapping needs to take all the above limitations into account.

5. Conclusions

In this study, we introduced the VFH as an innovative approach for the analysis of intracardiac signal propagation using matrix-like catheters and vector field theory. Our application of VFH in the context of scar-related VTs demonstrates its potential in enhancing the accuracy of identifying critical isthmus sites for catheter ablation. The mapping outcomes have shown a statistically significant increase in propagation heterogeneity at these sites compared to low voltage areas (LVAs) and normal voltage areas (NVAs), suggesting that VFH could be used for targeting ablation sites without the necessity of inducing ventricular tachycardia (VT). Looking ahead, further research will focus on integrating VFH into existing intracardiac mapping systems and assessing its applicability to other cardiac conditions, such as atrial fibrillation.

Acknowledgments

This project has been partially funded by the Ministry of Science and Innovation of the Government of Spain (PID2022-142514OB-I00), the Instituto de Salud Carlos III (CIBERCV CB16/11/00486) and the Generalitat Valenciana (PROMETEOII/2014/037).

References

[1] El Haddad, M., Houben, et al. Novel algorithmic methods in mapping of atrial and ventricular tachycardia. *Circulation: Arrhythmia and Electrophysiology*, 2014, 7(3), 463–472.

[2] Rohin K. Reddy, James P. Howard, et al. Catheter ablation for ventricular tachycardia after MI: A reconstructed individual patient data meta-analysis of randomised controlled trials. *Arrhythmia & Electrophysiology Review*, 2023;12

[3] Martin R., Hocini M., Haissaguerre M., Jaïs P., Sacher F. Ventricular tachycardia isthmus characteristics: Insights from high-density mapping. *Arrhythmia & Electrophysiology Review*, 2019.

[4] Guandalini G.S., Liang J.J., Marchlinski F.E. Ventricular tachycardia ablation: Past, present, and future perspectives. *JACC: Clinical Electrophysiology*, 2019 Dec.

[5] Deno D.C., Bhaskaran A., et al. High-resolution, live, directional mapping. *Heart Rhythm*, 2020.

[6] Castells F., Cervigón R., Millet J. On the preprocessing of atrial electrograms in atrial fibrillation: Understanding Botteron's approach. 2014 Feb.

[7] Ruipérez-Campillo, S., Crespo, M., et al. Evaluation and assessment of clique arrangements for the estimation of omnipolar electrograms in high-density electrode arrays: An experimental animal model study. *Physical and Engineering Sciences in Medicine*, 46(3), 1193-1204, 2023.

[8] Castells F., Ruipérez-Campillo S., et al. Performance assessment of electrode configurations for the estimation of omnipolar electrograms from high-density arrays. *Computers in Biology and Medicine*, 2023 Mar.

[9] Pancorbo L., Ruipérez-Campillo S., et al. Vector field heterogeneity for the assessment of locally disorganised cardiac electrical propagation wavefronts from high-density multielectrodes. *IEEE OJEMB*, 2023 Dec.

[10] Ganesan P., Deb B., et al. Quantifying a spectrum of clinical response in atrial tachyarrhythmias using spatiotemporal synchronization of electrograms. *Europace*, 2023.

[11] Ö. Özgül, et al. High-density and high coverage composite mapping of repetitive atrial activation patterns. *Computers in Biology and Medicine*, vol. 159, 2023 Jun.

Correspondence

Samuel Ruipérez-Campillo
ETH Zürich, Department of Computer Science,
CAB G 15.2, Universitätstrasse 6, 8092 Zürich,
Zürich, Switzerland